Volume 4, Issue 4(2016) 692-697 ISSN 2347 - 3258
International Journal of Advance Research and Innovation

Numerical Simulation of NACA 2415 Airfoil at Different Low Reynolds Numbers and Angles of Attack

Aakash Srivastava, Vatsalya Tiwari, Raj Kumar Singh
Department of Mechanical Engineering, Delhi Technological University Bawana Road, Delhi

Article Info
Article history:
Received 25 September 2016
Received in revised form
20 October 2016
Accepted 28 November 2016
Available online 15 December 2016

Keywords: Computational Fluid Dynamics (CFD), NACA2415, FLUENT, Spalart-Allmaras, Validation of results Effect of Reynolds number and Angle of Attack.

Abstract
This project simulates NACA2415 airfoil on ANSYS Workbench and ANSYS FLUENT at low Reynolds numbers at different angles of attack. This is a 2-D simulation andSpalart-Allmaras is the preferred turbulentmodel solver for this process, it yielded more results closer to experimental results when compared against K-epsilon and other turbulent models.Contours of Pressure and Velocity are presented in this paper with their inferences discussed while Plots of Coefficient of Pressure (C_P) about the chord lengths along the airfoil and Coefficient of Lift (C_L) are plotted to compare the CFD and the experimental results. Effect of Reynolds number and Angle of Attack is thus studied and investigated.

1. Introduction

Ever since the emergence of powerful computers and advanced numerical techniques and algorithms, computational fluid dynamics (CFD) has revolutionized aerospace industries all over the world. While experimental testing will always remain an integral part of the design, CFD is reducing the dependencies on experimental testing and has emerged as one of the important design tools for aerospace vehicle design [1]. Being cost-efficient, reliable and productive, CFD finds its usage in solving complicated problems, where testing experimentally in say, wind tunnels is difficult and expensive.

An **airfoil** or **aerofoil** is the shape of a wing or blade (of a propeller, rotor, or turbine) or sail as seen in cross-section. An airfoil-shaped body moved through a fluid produces an aerodynamic force. The component of this force perpendicular to the direction of motion is called lift. The component parallel to the direction of motion is called drag. Subsonic flight airfoils have a characteristic shape with a rounded leading edge, followed by a sharp trailing edge, often with a symmetric curvature of upper and lower surfaces. The lift on an airfoil is primarily the result of its angle of attack and shape. When oriented at a suitable angle, the airfoil deflects the oncoming air, resulting in a force on the airfoil in the direction opposite to the deflection. This force is known as aerodynamic force and can be resolved into two components: lift and drag [2].

2. Nomenclature

The shape of an airfoil is depicted in the Figure.1. The **leading edge** is the point at the front of the airfoil that has maximum curvature. The **trailing edge** is defined similarly as the point of maximum curvature at the rear of the airfoil. The **chord line** is a straight line connecting the leading and trailing edges of the airfoil. The *chord length* or simply **chord** is the length of the chord line and is the characteristic dimension of the airfoil section [3].

Hasanuzzaman Md, Mashud, Md. (2013), used FLUENT to see effect of Reynolds number on aerodynamic characteristics of NACA2415 airfoil with flap and they concluded flow separation can be controlled by using flap at maximum camber position [4].

Ghods, M. (2001) conducting an experiment to introduced the basic theory of wing and provide an introduction on wind tunnel testing involving NACA2415. Lift increases as the angle of attack increases, maximum liftis generated [5].

Ismail, Md. (2013), did investigation on the Aerodynamic Characteristics of NACA2415 airfoil at Reynolds number of 200000 and calculated Cd, Cl, Cp and discussed the formation of Laminar Separation Bubble [6].

Luis Velazquez-Araque and Jiří Nožička (2014), by means of CFD using k-epsilon model obtained lift, drag and pitching moment coefficients and also the flow field of air past airfoil 2415-3S.[7]

The aim of this research was to perform parametric investigate the aerodynamics characteristics of a NACA2415 airfoil system.

Computations were performed for various configurations of the system where each configuration represents a different Re number and angle of attack. The type of flow observed was subsonic and turbulent. Numerical simulations were focused on visualizing and analyzing pressure, velocity and lift of the airfoil system in steady state. Numerical simulations were performed using the hybrid grid Reynolds Averaged Navier-Stokes solver, ANSYS FLUENTTM. It is necessary to generate the computational grids and choose a computational turbulence model that could capture the complex flow phenomena around the airfoil. Initial studies were primarily focused on choosing the best turbulence model for the numerical simulations of the airfoil system. The turbulence model is critical to the computational solution and care must be taken to choose a model that can accurately compute and resolve the complex flow around the airfoil. Ideal and most accurate turbulence model was found out to be Spalart-Allmaras turbulent model. Other models, namely, K-Epsilon and K-Omega were also tested against it. Turbulence model validation was performed by computationally analyzing the NACA 2415 airfoil section and comparing the lift, drag, and pressure coefficient results with experimental data.

***Corresponding Author,**
E-mail address: rksingh.dtu@gmail.com; cheeku1612@gmail.com, atsalya.tiwari.vns@gmail.com,

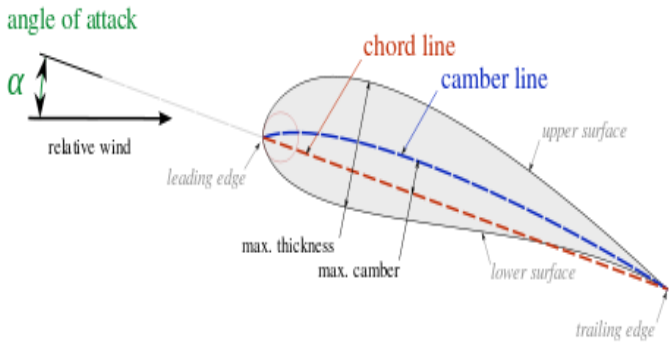

Fig.1 Nomenclature and shape of an Airfoil.[2]

2.1 Model

ANSYS FLUENT software could provide many turbulence models including Spalart-Allmaras model, k-model and the Reynolds stress model and K-Omega model, etc. Spalart-Allmaras turbulence model was put forward by S. Allmaras in 1992, which is a simple-equation turbulence model through solving the turbulence viscosity of the transport equations. It is the preferred model for the numerical simulations in this project. This turbulence model is a single-equation turbulence model applied to the turbulent flow along the solid wall boundary including the laminar flow, which has a smaller calculation, a good stability and a high precision.

The one-equation model is given by the following equation: [8]

$$\frac{\partial \hat{\nu}}{\partial t}+u_j\frac{\partial \hat{\nu}}{\partial x_j}=c_{b1}(1-f_{t2})\hat{S}\hat{\nu}-\left[c_{w1}f_w-\frac{c_{b1}}{\kappa^2}f_{t2}\right]\left(\frac{\hat{\nu}}{d}\right)^2+\frac{1}{\sigma}\left[\frac{\partial}{\partial x_j}\left((\nu+\hat{\nu})\frac{\partial \hat{\nu}}{\partial x_j}\right)+c_{b2}\frac{\partial \hat{\nu}}{\partial x_i}\frac{\partial \hat{\nu}}{\partial x_i}\right]$$

2.2. Grid Generation

The numerical simulation of airfoil NACA 2415 is performed using ICEM software to build the calculated model whose chord length is taken as unity. Computational solutions are sensitive to the discretization of the computational domain. For the present 2D computations, grids, as shown in Fig. 3, were generated with structured cells consisting of very fine quadrilateral elements in the boundary layer region of the airfoil and less dense cells consisting of quadrilateral elements for the rest of the domain. The computational domain is the geometrical region which bounds the numerical simulation. The distance of the far-field region from the surface of the airfoil must be such that the effects of the flow at the far-field region do not have an impact on the near-field solution. The computational domain area is determined by the far-field distance given in terms of the chord length of the airfoil under consideration. Figures 2.a and 2.b are views of grid generated for this problem, of airfoil and of entire domain respectively. Computational domain area for the present grids was defined by placing the far-field boundaries at 10 times the system chord length. The total grid consists of 40200 cells, 40602 nodes and 80802 faces.

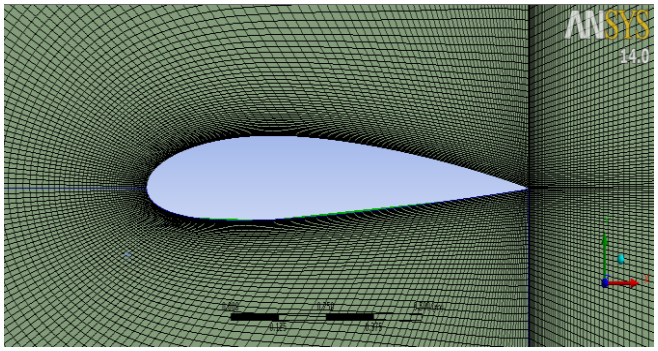

Fig. 2(a) Zoomed-in views of the airfoil mesh.

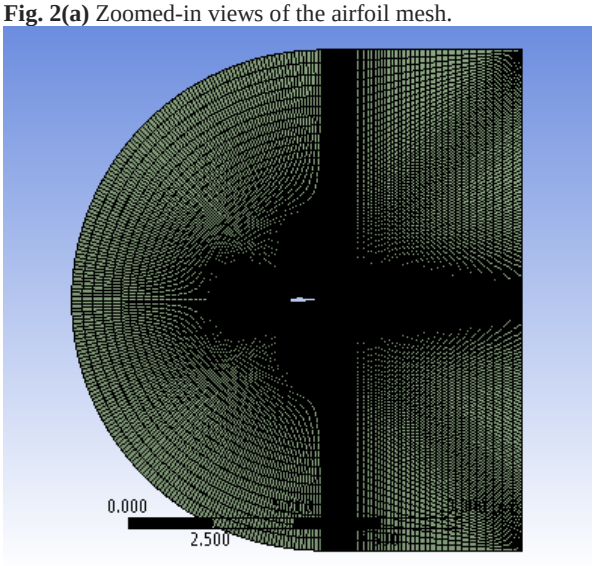

Fig. 2(b) Mesh of entire domain.

2.3. Inputs and Boundary Conditions

The problem considers flow around the airfoil at configurations of Angle of Attack (AOA) [0º, 4º, 8º, and 12º] and Re numbers [0.5 x 10^5, 1 x 10^5, and 2 x 10^5]. For that, some initial inputs and boundary condition are fed to the software and presented in the *Table 1*. Surface of airfoil is selected as a solid wall. The inlet boundary is given by using the free stream.

Table 1 Boundary conditions at the inlet.

S.no	Input	Value
1	Operating Temperature	288.16 Kelvin
2	Density of Fluid (air)	1.225 Kg/m3
3	Model	Spalart-Allmaras
4	Kinematic Viscosity	0.000177701
5	Length (Chord length)	1 m
6	Ratio of Specific Heats	1.4
7	Turbulent Intensity	0.3 %

2.4. Solver

All solutions in this study were computed using the Reynolds Averaged Navier-Stokes solution scheme. Numerical analysis was done using the density-based solver by applying the transport equations at the nodes of the grid elements. The inputs that have been specified to FLUENT for solving a problem are shown in *Table 2*. Convergence of solution varied in the different configurations, but the solution always converged in less than 2500 iterations in any of the cases.

Table 2. Inputs and Selections for this problem

S.no	Input	Selection
1	Type of solver	Density-based
2	Time	Steady
3	Formulation	Implicit
4	Gradient	Least Squares Based
5	Flow	Second Order Upwind
6	No. of Iterations	4000

3. Results

After successful calculations and results convergence, the graphs and contours were plotted and studied via *ANSYS CFD-POST*.

3.1 Grid Convergence

Grid convergence was checked via various grid sizes containing 10050 cells, 20100 cells, 40200 and 80400 cells respectively. Grid convergence was observed when the grid size consisted of 40200 cells.*Figure 3* represents a curve informing about the grid convergence in detail.

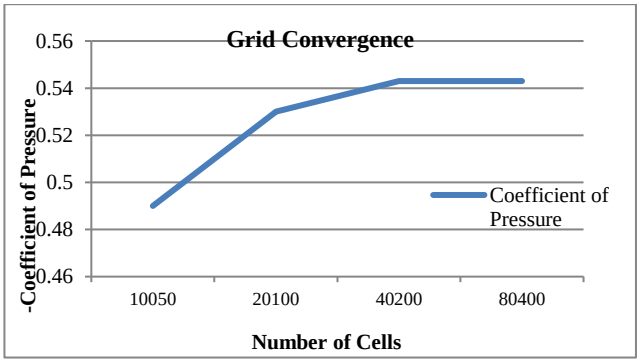

Fig. 3 Chart between values of –Cp obtained against the grid size. (Re = 2 x 105, Angle of Attack = 00 and Chord length = 0.2)

3.2 Pressure Contours

By the help of the Pressure contours from *Figures 4.a, 4.b* and *4.c*, it was observed that a region of high pressure was observed near the trailing edge on the lower surface and pressure gets reduced as we move away from the trailing edge along the surface. For zero angle of attack, there was less variation in pressure values at same chord lengths on the upper and lower surfaces. When the angle of attack is increased, more variation is observed in the respective values, lower surface pressures being considerably higher than the upper surface. As the Reynolds number is increased, pressure at all points also increases.

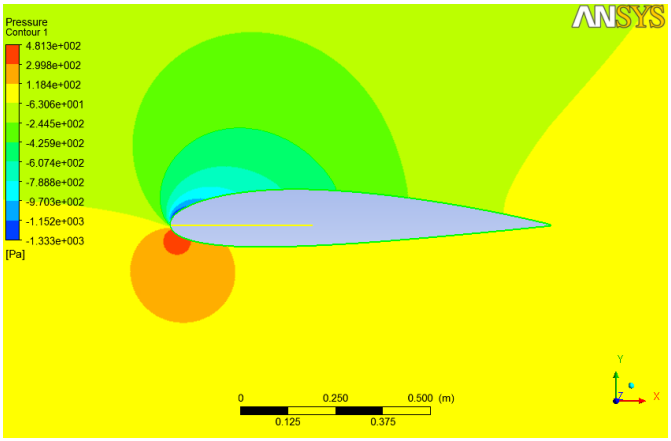

Fig. 4(a) Pressure contours across airfoil at Re=2 x $10^5$and Angle of Attack 12^0

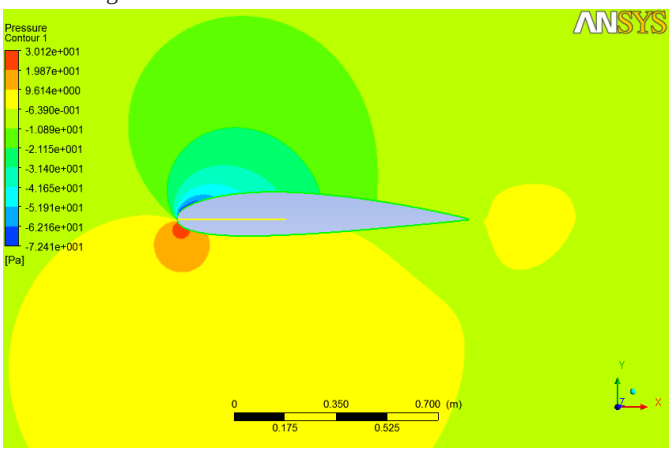

Fig. 4(b) Pressure contours across airfoil at Re = 0.5 x 10^5 and Angle of Attack 12^0

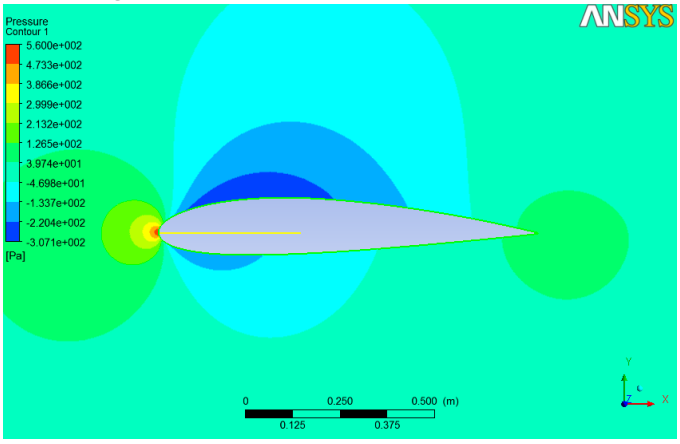

Fig. 4 (c) Pressure contours across airfoil at Re = 2 x 10^5 and Angle of Attack 0^0

3.3 Charts: Pressure v/s Chord length

Figures 5.a and *5.b* depict the definite value of pressure across the upper and lower surfaces of the airfoil. As said

above, when AOA was set to 0 degrees, there is significantly lesser difference between the pressures between upper and lower surfaces. At AOA = 12 degrees, pressure variation is observed to be maximum. Chord length of the airfoil is 1 unit (In this case, 1 metre).

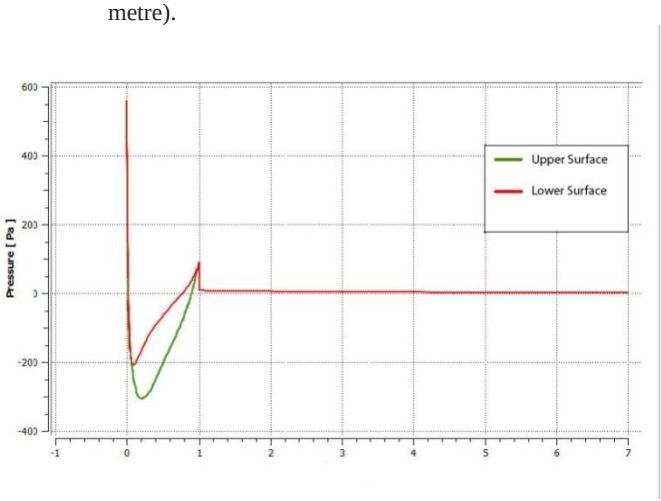

Fig. 5(a): Plot between Pressure and Chord length across Upper as well as Lower Surface of Airfoil (Re = 2 x 105, AOA = 00)

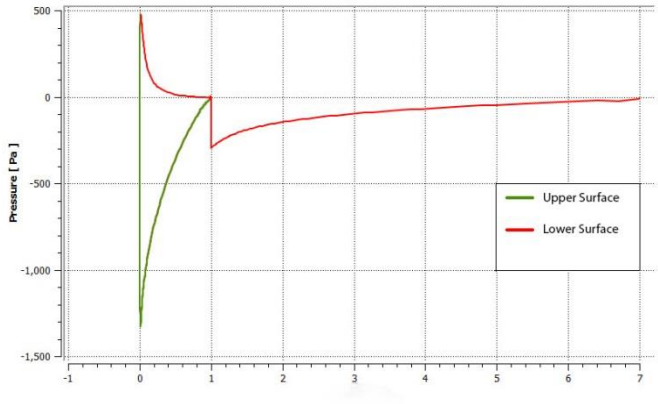

Fig.5(b) Plot between Pressure and Chord length across Upper as well as Lower Surface of Airfoil (Re = 2 x 105, AOA = 120.)

3.4 Velocity Contours

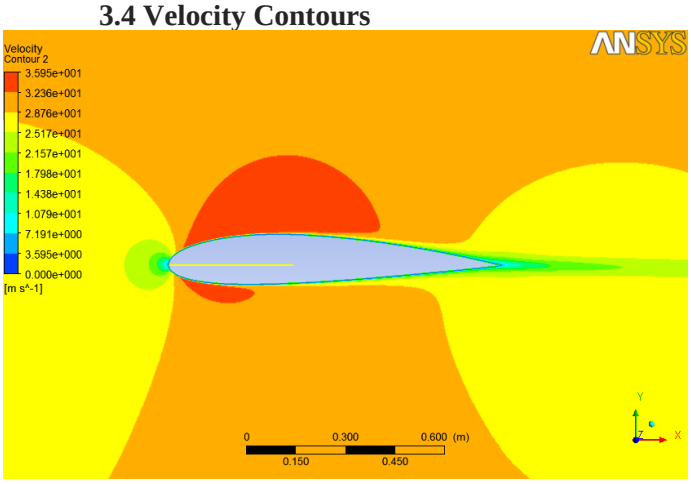

Fig. 6(a): Velocity contours across airfoil at Re = 2 x 10^5 and Angle of Attack 0^0

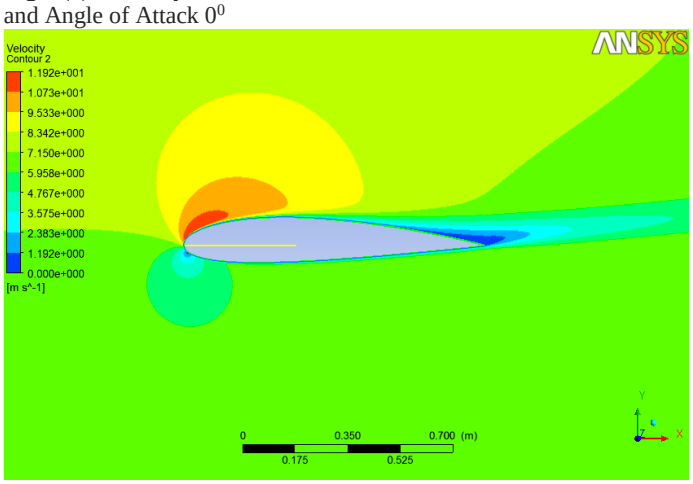

Fig. 6(b) Velocity contours across airfoil at Re = 0.5 x 10^5 and Angle of Attack 12^0

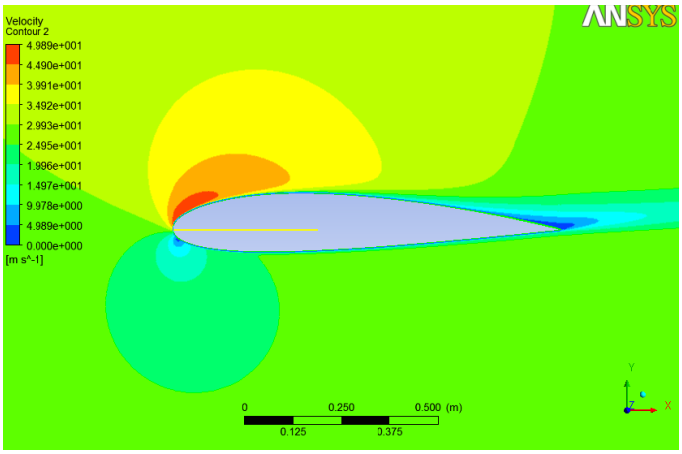

Fig. 6(c): Velocity contours across airfoil at Re = 2 x 10^5 and Angle of Attack 12^0

By the help of the velocity contours from Figures 6.a, 6.b and 6.c, it was observed that a region of high velocity was observed near the trailing edge on the upper surface and velocity gets reduced as we move away from the trailing edge along the surface. For zero angle of attack, there was less variation in velocity magnitudes at same chord lengths on the upper and lower surfaces. When the angle of attack is increased, more variation is observed in the respective values, lower surface pressures being considerably lower than the upper surface. As the Reynolds number is increased, velocity at all points also increases.

3.4 Comparison between Different Models

Figure 7. represents a chart where the experimental data, and CFD results obtained by both Spalart Alramus and K-Epsilon Methods are plotted together for observation and to draw out inferences.

It can be observed that the coefficient of pressure obtained when method Spalart Allmaras is chosen proves to be better and more accurate when compared against the method K-epsilon. Results obtained by Spalart Allmaras method show close resemblence to the values obtained by the experiement and also follow the trend of the experimental data curve.

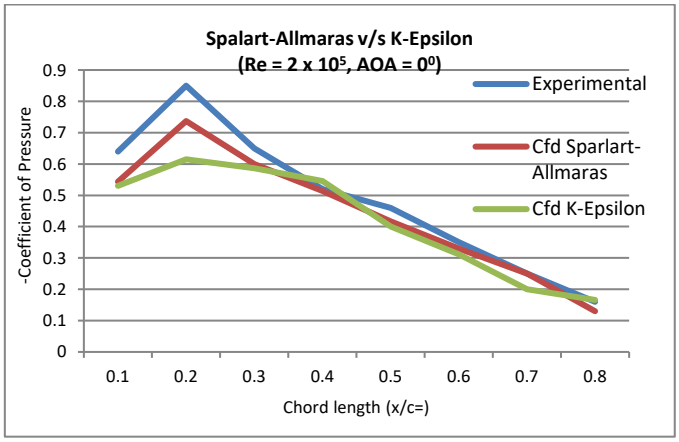

Fig.7 Chart for comparison of results of Spalart-Allmaras and K-Epsilon methods with experimental data

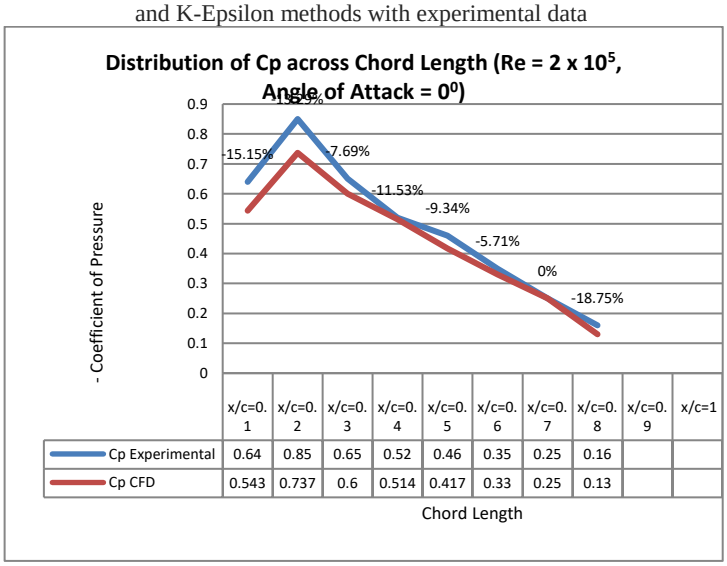

	x/c=0.1	x/c=0.2	x/c=0.3	x/c=0.4	x/c=0.5	x/c=0.6	x/c=0.7	x/c=0.8	x/c=0.9	x/c=1
Cp Experimental	0.64	0.85	0.65	0.52	0.46	0.35	0.25	0.16		
Cp CFD	0.543	0.737	0.6	0.514	0.417	0.33	0.25	0.13		

Fig. 8(a) Chart between –CP (Coefficient of Pressure) and Chord length for Reynolds number = 2 x 10^5 and Angle of attack = 00. Experimental Data as well as CFD results are plotted together (% Deviations mentioned in the graph)

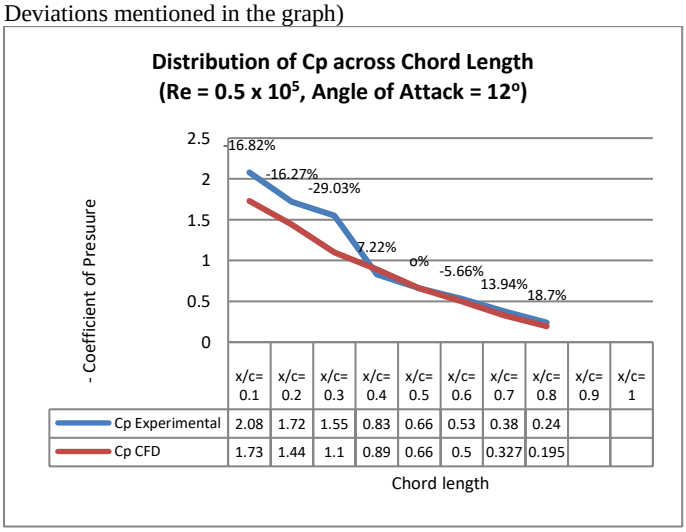

	x/c=0.1	x/c=0.2	x/c=0.3	x/c=0.4	x/c=0.5	x/c=0.6	x/c=0.7	x/c=0.8	x/c=0.9	x/c=1
Cp Experimental	2.08	1.72	1.55	0.83	0.66	0.53	0.38	0.24		
Cp CFD	1.73	1.44	1.1	0.89	0.66	0.5	0.327	0.195		

Fig. 8(b) Chart between –CP (Coefficient of Pressure) and Chord length for Reynolds number = 0.5 x 105 and Angle of attack = 120. Experimental Data as well as CFD results are plotted together (% Deviations mentioned in the graph).

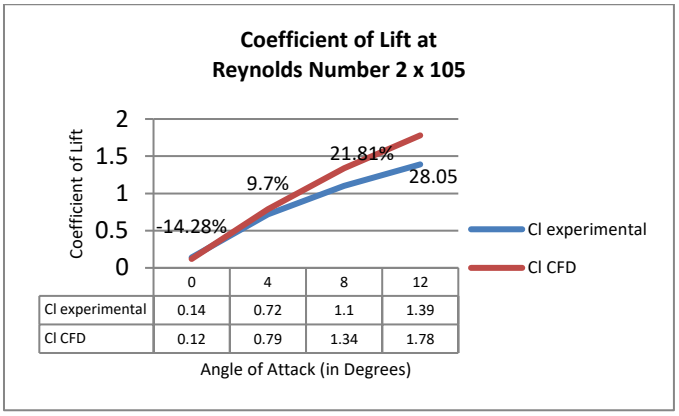

	0	4	8	12
Cl experimental	0.14	0.72	1.1	1.39
Cl CFD	0.12	0.79	1.34	1.78

Fig. 8(c) Chart between –CL (Coefficient of Lift) and Angle of Attack for Reynolds number = 2 x 105. Experimental Data as well as CFD results are plotted together (% Deviations mentioned in the graph)

3.5 Comparison of Results obtained with Experimental Data

The results obtained were compared to the experimental results of a research experiment conducted by University of Ecylies[9], on the same airfoil and similar conditions in a wind tunnel. The comparison as shown in Figures 8.a, 8.b and 8.c, showed close resemblence thus validating this research. Hence, the results of this experiment can be used for further investigations and experiments.

4.Conclusions

This project simulates NACA2415 airfoil on ANSYS FLUENT at low Reynolds numbers at different angles of attack. With Spalart-Allmaras as the preferred turbulent model, results were calculated and analyzed. Contours of Pressure, Velocity were presented and Coefficient of Pressure, Lift were compared against the experimental values. The following conclusions can be considered.

- Most appropriate turbulent model for this simulation found out to be Spalart-Allmaras Turbulent model when tested against other turbulent models such as k-epsilon. It yielded more accurate results.
- Contours of Pressure and Velocity show that parameters of Pressure and Velocity are greatly influenced by Reynolds number and Angle of Attack.
- Coefficient of Pressure (CP) and Coefficient of Lift (CL) were calculated and compared with the experimental values which showed close resemblance thereby, validating this research.

This study can further be optimized by testing it in unsteady states and on a wider range of angle of attack and Reynolds numbers.

References

[1.] SinghK.P, Mathur, JS, Ashok, V, Chakraborty D., Computational Fluid Dynamics in Aerospace Industry in India, Defence Science Journal, 60(6), 2010, 639-652.

[2.] Airfoil Nomenclature, Images, Wikipedia, http://en.wikipedia.org/wiki/Airfoil

[3.] 'Airfoil', Wikipedia, http://en.wikipedia.org/wiki/Airfoil\

[4.] Hasanuzzaman, Md. and Mashud, Md., Effect of Reynolds Number on Aerodynamic Characteristics of an Airfoil with Flap, Annals of Pure and Applied Mathematics, 3(1), 2013, 27-40.

[5.] Ghods M, Theory of wings and wind tunnel testing of a NACA 2415 airfoil, Technical Communication for Engineers, The University of British Columbia, 23, 2001.

[6.] Bin Ismail Md, Parametric investigation on the aerodynamic characteristics of NACA2415 airfoil at low Reynolds number, Faculty of Manufacturing Engineering, University of Malaysia, Pahang, 2013.

[7.] Velazquez-Araque1 L, Nožička J. Computational Analysis of the 2415-3S Airfoil Aerodynamic Performance, Systemics, Cybernetics and Informatics 12(1), 2014.

[8.] Turbulence Modeling Resource, Langley Research Center'; http://turbmodels.larc.nasa.gov/spalart.html

[9.] Serdar Genç, M., Karasu, I., Hakan Açıkel, H., 'An experimental study on aerodynamics of NACA2415 aerofoil at low Re numbers', M.S. Genç et al./ Experimental Thermal and Fluid Science 39, 2012, 252–264.